Environmental Engineering and Management Journal *September 2019, Vol.18, No. 9, 2055-2061*
http://www.eemj.icpm.tuiasi.ro/; http://www.eemj.eu

"Gheorghe Asachi" TechnicalUniversity of Iasi, Romania

PROPAGATION CHARACTERISTICS AND ENVIRONMENTAL IMPACT OF COAL DUST EXPLOSION

Baichao Song[1,2], Yucheng Li[3]*

[1]College of Safety Science and Engineering, Liaoning Technical University, Fuxin 123000, China
[2]Key Laboratory of Mine pressure, Hulunbuir 023008, China
[3]College of Safety and Emergency Management Engineering, Taiyuan University of Technology, Taiyuan 030000, China

Abstract

Dust explosions are one of the main causes of mining disasters. To avoid them, it is important to understand how they are propagated. In the study reported here, computational fluid dynamics software was used to model a 3D diagonal pipe network then simulated a dust explosion at its inlet to examine its propagation characteristics. The initial conditions, boundary conditions and parameter settings were detailed description in the simulation to analyze possible propagation characteristics, assessing in particular the flame temperature, concentration of the produced CO and airflow velocity after the explosion. Our findings suggest that when dust explosions propagate in a straight pipe, the highest flame temperature is almost at the center of the pipe. When the pipe is bifurcated, the flame propagation is disrupted by turbulence and the gravity of the coal dust particles generated by the combustive reaction at the flame front. In line with the position of the flame front and the gravity of the coal dust, the production of explosion-related CO is more concentrated in the lower part of the pipe, along the section vertical to the x-axis. The shock airflow generated by coal dust explosion propagates much faster at the forks and bends in the pipes, because these structures work in the same way as obstacles in a straight pipe, bringing about an "excitation effect", which significantly increases the impact of the airflow velocity.

Key words: computational fluid dynamics (CFD) simulation, dust explosion, diagonal pipe network, environmental effect, propagation characteristics

Received: March, 2019; Revised final: April, 2019; Accepted: May 2019; Published in final edited form: September, 2019

1. Introduction

Dust explosions are one of the five main causes of disasters in mines. The high temperature flames, shock waves and poisonous gases generated by such explosions can seriously injure or kill underground workers and cause huge economic losses (Cao et al., 2017; Ghicioi et al., 2017). To prevent such incidents and develop emergency response plans against them, it is vital that the propagation characteristics of dust explosions be properly understood.

The characteristics of dust explosions can be affected by a range of factors, including dust concentration, particle size, dispersion and coal quality. The propagation patterns are also different in different spaces (Suvar et al., 2017). Ajrash et al. (2016) put methane and coal dust in a large cylindrical explosion chamber and studied the effects of ignition energy on the explosion's overpressure of the mixture. Li et al. (2016) studied the effect of particle size and particle size dispersion on the intensity of dust explosions by measuring the maximum pressure and its rate of increase in a 20 L spherical explosion vessel. Cao et al. (2017) studied the intensity of dust explosions by using both a 20 L spherical vessel test and numerical simulation. From this they obtained the relationship between the explosion's pressure and rate of pressure rise and the coal dust concentration and ignition delay. They also found that their simulation results were consistent with the results of their actual tests. Li et al. (2015a, b; 2017a, b, c, d) studied dust explosions across a range of experiments in a 20 L

* Author to whom all correspondence should be addressed: e-mail: lyclntu@163.com; Phone: +86-13841826164

sphere and small-scale horizontal glass tubes to analyze length of flames produced by dust explosions and the factors influencing this. Jing and Yang (2010) studied the propagation characteristics of dust explosions with a self-designed experimental device consisting of an explosion chamber (1.5 m long and 0.3 m in diameter) and a square section of pipe (80 mm × 80 mm). This enabled them to examine the propagation patterns in a dust explosion's flame zone, the resulting shock waves and the presence of poisonous gases. Li (2010, 2013) have also studied the propagation patterns of gas and dust explosions using numerical simulations.

In summary, most research regarding dust explosions is based on experiments, with the experimental vessels chiefly being 20 L spheres and small-scale experimental pipelines. To date, very little research has been done on the propagation characteristics of dust explosions in a network of pipes, despite the fact that the statistics from dust explosion incidents indicate that the explosions may be more severe in diagonal pipe networks. Some research (Cheng et al., 2018; Song and Li, 2018) has undertaken numerical simulation of dust explosions in a diagonal network and obtained various patterns regarding temperature, airflow velocity and pressure after an explosion in a diagonal branch, but there was no consideration of the possible influence of coal dust gravity on the explosion's characteristics. In view of the complexity of large diagonal networks and the significant difficulty of monitoring CO concentration in real-time, computational fluid dynamics (CFD) software was used to establish a 3D diagonal pipe network model and simulated a dust explosion at the inlet of the pipe network.

The propagation patterns were then analyzed in relation to airflow, flame temperature and CO concentrations, taking into account the potential influence of coal dust gravity upon the explosion's characteristics (Benyoucef et al., 2017; Camaraza-Medina et al., 2018; Dahham et al., 2018; Moldovan et al., 2017; Si, 2011; Yang et al., 2010).

2. Materials and methods

2.1. Geometric modeling of the diagonal network and the grid meshing

A 3D geometric model of a diagonal pipe network was drawn and meshed using the geometry and mesh generation software for CFD, GAMBIT, as shown in Fig. 1.

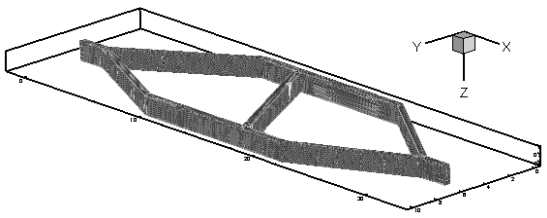

Fig. 1. Geometric model of the diagonal network

The model was about 32 m long and 10 m wide, with a height of 0.5 m. The diagonal branch branches were about 10 m long. The model was divided into Tet/Hybrid (tetrahedron/hybrid) grids using TGrid, which is dedicated pre-processing software for fluid flow analysis. The total number of grids was 140,560.

2.2. Setting of initial conditions, boundary conditions and model parameters

2.2.1. Setting of initial conditions

(1) Initial pressure: One standard atmosphere 0.1 MPa.

(2) Initial velocity: The initial velocity at the entrance of the flow field was 4 m/s, with the airflow into each branch of the diagonal network conforming to a natural distribution of airflow.

(3) Initial temperature: The initial temperature in the ignition zone was 1500 K, with that of the non-ignition zone and the inner wall of the pipe being 300 K.

(4) Initial incident conditions for the dispersion of coal dust particles: The plane of incidence was the velocity inlet plane and the initial temperature of the incident particles was 300 K. The initial direction of the particles was positive along the x-axis and the initial velocity of the particles was 4 m/s.

(5) Initial high temperature ignition zone: The area formed by the sections x=0.5 and x=1 was the high temperature ignition zone in the pipe, with a temperature of 1500 K and with a duration of 1 s. The mass fraction of O_2 in this zone was 23%, of H_2O it was 0.01% and of CO_2 0.01%.

(6) Action of gravity: the gravitational acceleration was 9.8 m/s^2 along the positive direction of the z-axis.

2.2.2. Setting of boundary conditions

The boundary conditions for the inlet and the outlet of the pipe network are shown in Table 1.

At the iron pipe wall, the density of the wall was 8,030 kg/m^3, the specific heat was 502 J/(kg·K), the thermal conductivity was 16.27 W/(m·K) and the roughness of the inner wall was 0.5. The boundary formed by the pipe wall being hit by particles can be considered the reflection boundary.

2.2.3. Setting of model parameters

The explosive particles were flammable and highly volatile 75 μm lignite dust, with a moisture content of 4.17%. The particle size dispersion conformed to the Rosen-Rammler distribution function. The interaction between the coal dust particles themselves is not considered here. The physical parameters of the combustible coal dust are given in Table 2.

The proportion of heat absorbed by the solid wall out of the heat released by coal dust combustion was set to 2%. In the stochastic particle tracking model for coal dust, the time-scale constant is 0.05 s and the frequency is 10, so, the incident time for coal dust particles is 0.5 s.

Table 1. Inlet and outlet boundary conditions

Condition / Setting / Boundary type	Relative pressure /Pa	Velocity m/s	Turbulence intensity /%	Hydraulic diameter /m	Temperature /K	O_2 mass fraction /%	Bc type
Speed at entrance		4	12	0.25	300	23	Escape
Pressure at outlet	0		10	0.25	300	23	Escape

Table 2. Physical properties of the combustible particles

Density /kg·m^{-3}	Cp /J·(kg·K)$^{-1}$	Volatile matter /%	Vaporization Temperature /k	Binary Diffusivity /m^2·s^{-1}	Swelling Coefficient	Burnout Stoichiometric	Combustible Fraction /%	Heat of Reaction for Burnout / J·kg^{-1}
1000	1100	36.88	773	3×10^{-5}	2	2.67	36.7	3.29×10^{7}

The maximum number of tracking steps is 20000 and the tracking step length 0.0025 m, so, the total tracking length for coal dust particles is 50 m. When the continuous phase is iterated by twenty steps, the discrete phase is iterated by one step. Outside of this, if it is supposed that the coal dust concentration of the explosion is 500 g/m^3, the incident mass flow rate = the particle cloud mass concentration × volume flow rate = $0.5\times(4\times0.5^2) = 0.5$ kg/s (the volume flow rate is the product of the incident velocity and the cross-sectional area).

The eddy dissipation model was selected as the coal dust particle combustion model and a two-step reaction mechanism was adopted, as Eqs. (1-2.)

$$h_v\text{-}vol + O_2 \rightarrow CO + CO_2 + H_2O + N_2 \quad (1)$$

$$O_2 + 2CO = 2\,CO_2 \quad (2)$$

The intermediate product of a dust explosion is CO, the end products CO_2, H_2O and N_2, with the explosion-supporting component being O_2. If the reaction is incomplete, the toxic gas CO will be generated. Further theoretical models regarding the propagation characteristics of dust explosions, such as the gas phase turbulence model, the gas phase turbulent combustion model, the coke combustion model, and the radiation model, can be found in Song. A principle of coupled calculation is adhered to here, which involves alternately calculating the continuous phase and the discrete phase flow fields. The discrete phase will change the mass, momentum, temperature and other information in the continuous phase, while the calculation results of the continuous phase will change the physical information relating to the discrete phase particles.

3. Results and discussions

3.1. Analysis of the propagation characteristics of the flame temperature

Fig. 2 shows the simulation results of the flame temperature propagation for a cross-section of z=0.25 at different times after the dust explosion (unit: K). From the flame temperature distribution nephogram at different times, it can be seen that 0.2 s after the incidence of coal dust from the velocity inlet, a point explosion of coal dust is initiated in the high temperature zone. The flame temperature then continues to propagate along the pipeline. The maximum temperature (3200 K) appears in the ignition zone at the instant of the point explosion, i.e. 0.5-1 m at 0.2 s. After that, the flame propagates outward, the flame temperature decreases and the highest flame temperature remains on the flame front. At 0.4 s, the flame reaches the fork of the pipeline. Due to the increase in local turbulence, the explosive reaction is excited. The maximum temperature (T_{max}=3000 K) thus rises from the maximum (T_{max}=2900 K) at 0.3 s. After the bifurcation, the heat spreads along the two branches and the flame temperature decreases again.

The flame temperatures for different sections along the x-axis at T=0.8 s are shown in Fig. 3. It can be seen that in the 0-2 m linear pipe section, the flame temperature is highest at the center of the pipe. However, after the bifurcation, moving to the section where x=6, the flame propagation starts to become disordered. The flame temperature is no longer highest at the center, but rather varies irregularly throughout the section. There are two reasons for this: 1) the turbulence at the fork of the pipeline leads to a severe local reaction, and 2) the coal dust particles still burning in the flame front are moving downward along the +z-axis due to gravity.

3.2. Analysis of the propagation characteristics of the toxic CO in a full explosive reaction

The CO mass fraction (%) distribution at t=0.5 s for the cross-section at z=0.25 is shown in Fig. 4. Examining the results here, it can be seen that the propagation over distance of the CO produced by the explosion followed much the same pattern as the flame temperature, i.e. the area where the CO was located was basically at the flame front.

The section where x=0.4~1.0 m was the spatial range with the highest CO mass fraction in the pipe body. The local maximum reached about 0.018%, indicating that the dust explosion reaction consumed more O_2 in this space.

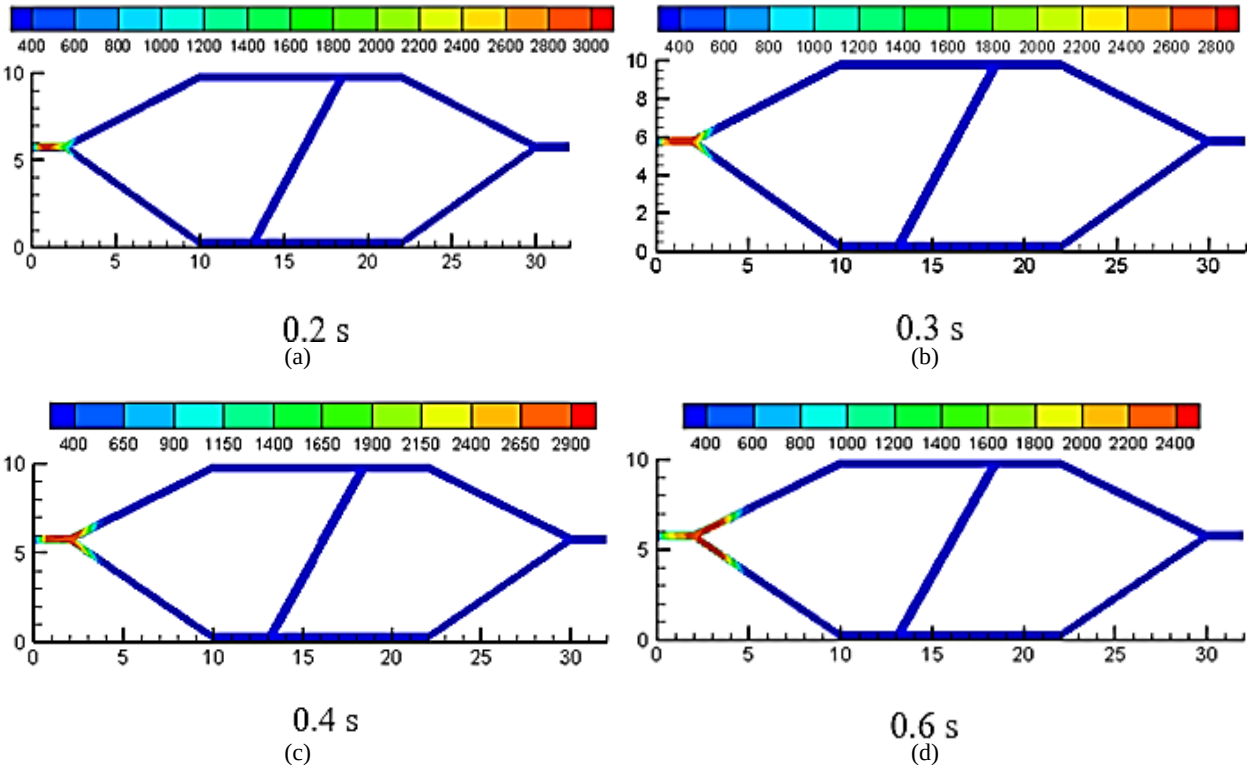

Fig. 2. Flame temperature distribution nephogram for the cross-section at z=0.25 at different times: (a)t=0.2s (b)t=0.3s(c)t=0.4s(d)t=0.6s

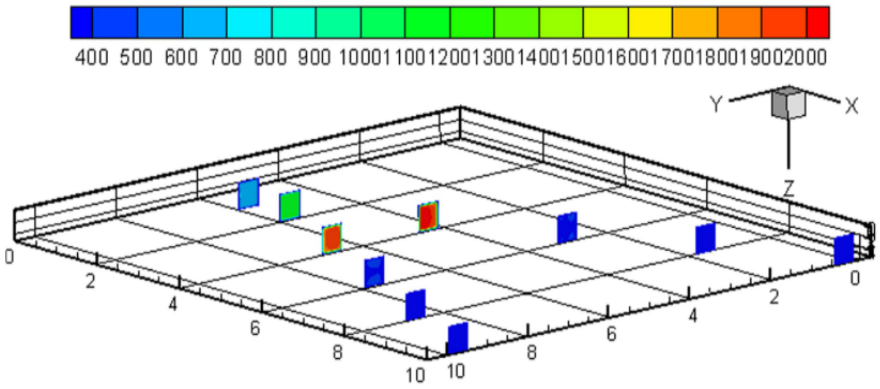

Fig. 3. Flame temperature chart for different sections along the x-axis

This is directly related to x=0.5~1.0 m being the highest temperature ignition zone. When x>1 m, moving farther away from the source of the explosion, the CO mass fraction reduces. At the fork, due to local turbulence, the CO concentration increases locally. For the range 0-2 m, the CO concentration is highest at the center of the pipe.

Fig. 5 is a nephogram of the CO mass fraction (%) at different distances along the x-axis (x=1 m, x=2 m, x=4 m and x=6 m) at 0.5 s and 0.9 s. Note that the areas around the centers of the sections at x=1 m and x=2 m were regions with a large CO mass fraction. This is consistent with the previous analysis that the maximum concentration was at the center of the pipe.

At t=0.5 s, the CO concentration at x=4 m began to diverge from the center of the pipe. This is the state of CO concentration for the section at x=4 m shown in Fig. 4(a). The reason for this was that the coal dust particles were starting to sink under the action of gravity at this time, concentrating the explosive reaction in the lower part of the pipe body. This resulted in there being insufficient oxygen in this area, leading to a further oxygen-deficient reaction. Thus, the combustion of coal dust particles was dominated by the first step in the two-step reaction mechanism, resulting in a larger CO mass fraction. At the same time, part of the CO in the original airflow tended to go upward because its density is smaller than the air and CO_2.

At t=0.9 s, the overall CO concentration had decreased still further from the concentration at 0.5 s. The CO was propagated up to x=6 m, along with the

flame front, and the CO mass fraction in the lower part of the pipe body was significantly greater than in the upper part, indicating that the coal dust particles were being more significantly affected by gravity. The combustive reaction was concentrated in the lower part of the pipe body. At the same time, the original CO in the upper part was further oxidized into CO_2 in the oxygen-rich environment.

3.3. Analysis of the impact of the dust explosion on the airflow velocity

A dust explosion generates a large number of products and the high temperature makes the products of the explosion expand rapidly, moving at high speed and producing a shock airflow. This has an impact on the airflow.

The airflow velocity nephogram for the cross-section at z=0.25, where t=0.8 s, is shown in Fig. 6. From this, it can be seen that the airflow propagated much faster at the forks and bends, mainly because these structures act in the same as obstacles in a straight pipe. The forks and bends changed the direction of the propagated airflow, bringing about an obvious "excitation effect" and sharply increasing the impacted airflow's velocity. At the junction of the uphill pipe and the diagonal branch, the velocity of the airflow significantly increased as the explosion propagated through the diagonal branch from the downhill space to the uphill one.

Note that the velocity of the airflow also significantly increased at the junction of the two parallel pipes at the right-hand end of the cross-section at z=0.25. This trend was still evident at the end of the manifold pipe. From the airflow velocity nephogram for the different sections along the x-axis, it can be seen that the velocity was not at its highest in the center of the pipe. At x=2 m where the pipe bifurcated, the airflow experienced significant turbulence, disrupting the previously smooth flow. The airflow velocity in this section thus started to show irregular variation. When the airflow reached the section at x=10, there were bends in the upper and lower pipelines, so the airflow impacted upon the external wall of the pipe. Under the action of inertia, this made the velocity adjacent to the wall decrease, while the more general airflow velocity inside the pipe continued to increase.

4. Conclusions

(1) When coal dust is ignited and explodes at the inlet of a diagonal pipe network, a large amount of CO is generated. The mass fraction of the CO is at its highest in the ignition zone, with the local maximum reaching about 0.018%. Outside the ignition zone and farther away from the explosion's source, the CO mass fraction is reduced. Generally speaking, the greatest concentration of CO is at the center of the pipe.

When x>4 m, the explosive reaction in the pipe body is mainly concentrated in the lower region because of the effect of gravity on the coal dust. This results in an oxygen-deficient reaction and a greater CO mass fraction, manifested by a larger concentration of CO in the lower part of the pipe.

(2) After the point where a coal dust explosion has occurred, the maximum flame temperature appears in the ignition zone at the instant of the explosion. The flame then propagates outward and the flame temperature decreases, with the highest flame temperature appearing on the flame front. However, at forks, due to the increase of local turbulence, the explosive reaction becomes excited. At this point, the temperature increases once more. After a bifurcation, the heat spreads along both of the bifurcated branches and the flame temperature starts to decrease again. In straight pipe sections, the flame temperature is at its highest in the center of the pipe.

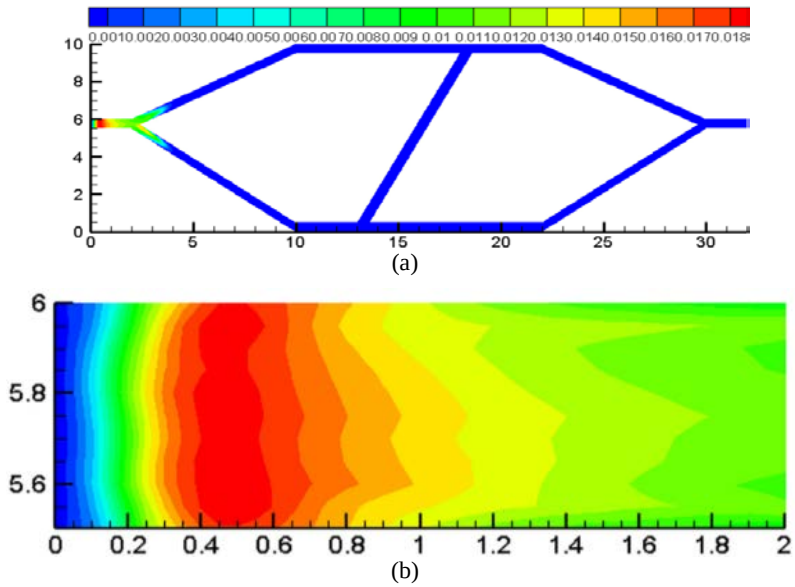

Fig. 4. CO mass fraction nephogram: (a) CO mass fraction nephogram for the cross-section at z=0.25m (b) local amplification in the range 0-2 m

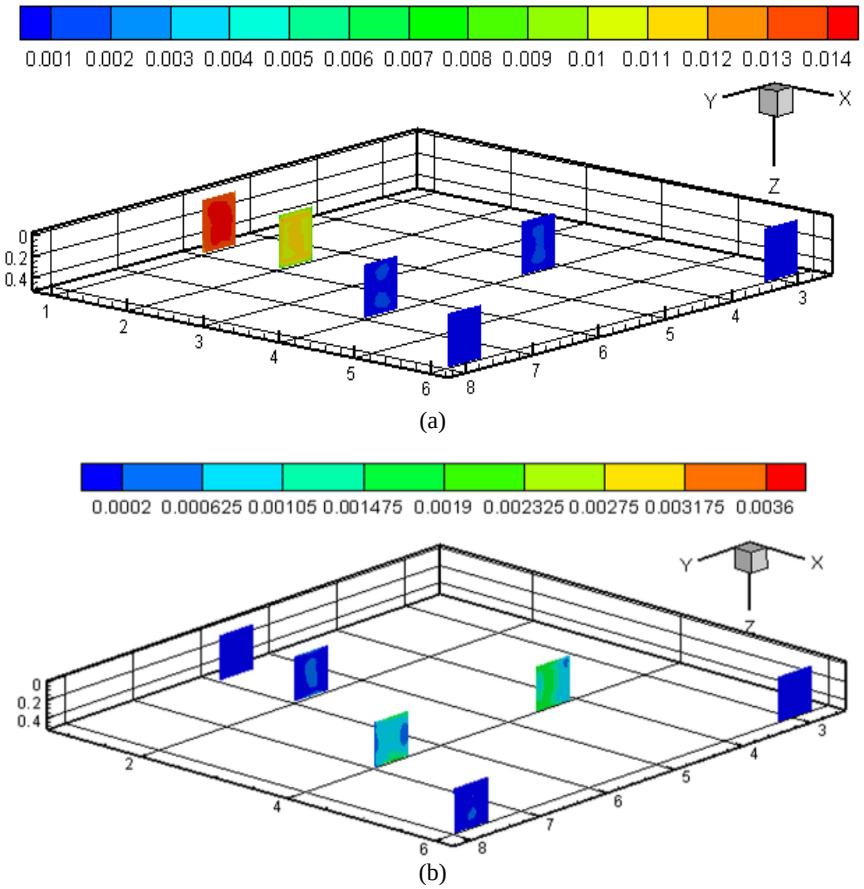

Fig. 5. CO mass fraction nephogram for different sections along the x-axisat 0.5 s and 0.9 s: (a) at t=0.5s(b) at t=0.9s

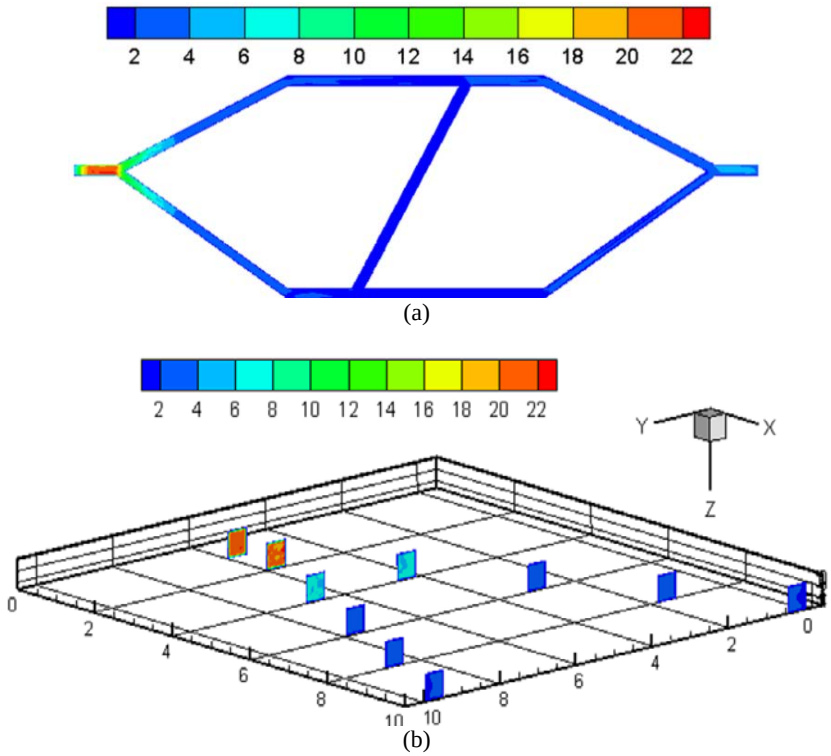

Fig. 6. Airflow velocity nephogram for different sections at t=0.8 s: (a) Cross-section at z=0.25; (b) Different sections along the x-axis

After a bifurcation, however, the flame propagation starts to become disordered and the flame temperature is no longer necessarily at its highest at the center, but rather varies in an irregular fashion.

(3) The airflow impacted by a dust explosion propagates much faster at forks and bends, because such structures are equivalent to obstacles in a straight pipe, bringing about the "excitation effect" noted above. This can lead to a significant increase in airflow velocity.

(4) The numerical simulation approach adopted in our study obviates the need to collect products from dust explosions and perform real-time monitoring during physical experiments, especially the monitoring of CO distribution along the x-axis. The simulation results are particularly instructive for the ongoing study of the propagation characteristics of dust explosions and their consequences. It should be noted, however, that the maximum flame temperature indicated by the simulation is higher than suggested by previous theoretical and experimental work. This is almost certainly related to the simplified assumptions selected for the model and the setting of some of the empirical constants. It is therefore clear that further development is required to make the model fully robust.

Acknowledgements

This work was supported by the Chinese National Natural Science Foundation (grant number 51774168) and Inner Mongolia Education Department Fund (grant number NJZY14306). We thank to Professor Yucheng Li for his guidance on this article.

References

Ajrash M.J., Zanganeh J., Moghtaderi B., (2016), Methane-coal dust hybrid fuel explosion properties in a large scale cylindrical explosion chamber, *Journal of Loss Prevention in the Process Industries*, **40**, 317-328.

Benyoucef D., Zeroual M., Benmoussa H., (2017), Natural convection in tilted rectangular cavities due to bidirectional temperature gradient, *International Journal of Heat and Technology*, **35**, 883-892.

Camaraza-Medina Y., Rubio-Gonzales Á.M., Cruz-Fonticiella O.M., García-Morales O.F., Vizcón-Toledo R., Quiza-Sardiñas R., (2018), Simplified analysis of heat transfer through a finned tube bundle in air cooled condenser-second assessment, *Mathematical Modelling of Engineering Problems*, **5**, 365-372.

Cao W.G, Qin Q.F, Cao W., (2017), Experimental and numerical studies on the explosion severities of coal dust/air mixtures in a 20-L spherical vessel, *Powder Technology*, **310**, 17-23.

Cheng P., Zhang J.H., Bai D., (2018), Establishment and optimization of fluid pipe network models based on topological analysis algorithm, *International Journal of Heat and Technology*, **36**, 1388-1392.

Dahham R.Y., Alkhafaji D., Al-Jelawy H., Hadi S.J., (2018), Experimental and numerical study of the effect of vibration on airflow between can combustor liner and casing, *Instrumentation Mesure Métrologie*, **17**, 235-257.

Ghicioi E., Gaman G.A., Vlasin N., Pasculescu V.M., Gabor D., (2017), Prevention of accidental pollution with combustion gases after the occurrence of explosions, *Environmental Engineering and Management Journal*, **16**, 1289-1294.

Jing G.X., Yang S.Z., (2010), Experimental study on propagation characteristics of coal dust explosion, *Meitan Xuebao/Journal of the China Coal Society*, **35**, 605-608.

Li R.Z., (2010), Numerical simulation of coal dust explosion induced by gas explosion, *Explosion and Shock Waves*, **30**, 529-534.

Li R.Z., (2013), Simulation study on propagation law of different - amount deposited coal dust explosion induced by gas explosion, *Mining Safety & Environmental Protection*, **40**, 17-25.

Li Y.C., Liu T.Q., Chen S.L., Liu J., Guo K.J., (2015a), Principal component analysis of the influence of coal quality index on the length of coal dust explosion flame, *Journal of Safety Science and Technology*,**11**, 40-45.

Li Y.C., Liu T.Q., Zhou X.H., (2015b), Study on combined prediction of flame propagation characteristics in coal dust explosion based on factors analysis and BP network, *China Safety Science Journal*, **25**, 53-58.

Li Q.Z, Wang K., Zheng Y.N., (2016), Experimental research of particle size and size dispersity on the explosibility characteristics of coal dust, *Powder Technology*, **292**, 290-297.

Li Y.C., Bi Q.P., Liu T.Q., (2017a), Study on flame features of coal dust explosion under coordinated role of mixed coal qualities, *Coal Science and Technology*, **45**, 68-71.

Li Y.C., Liu T.Q., Zhao X.T., (2017b), Experimental study on bituminous coal dust explosibility influence factors, *Journal of Liaoning Technical University (Natural Science)*, **36**, 354-358.

Li Y.C., Liu T.Q., Zhou X.H., Chu Y., Meng Y., (2017c), On the characteristic influential factors of the coal dust explosion flame propagation via the small-scale horizontal glass tube, *Journal of Safety and Environment*, **17**, 2176-2179.

Li Y.C., Liu T.Q., Zhou X.H., Liu R.Z., (2017d), Flame characteristics of deposited coal powder explosion induced by high-pressure airflow carrying coal dust, *Journal of Liaoning Technical University (Natural Science)*, **27**, 58-63.

Moldovan L., Burian S., Magyari M., Darie M., Fotau D., (2017), Factors influencing the determination of maximum surface temperature for explosion-proof luminaires, *Environmental Engineering and Management Journal*, **16**, 1309-1316.

Si R.J., (2011), Simulation Research of Gas Concentration on Explosion Propagation. -Industrial Safety and Environmental Protection, **37**, 29-30.

Song B.C., Li Y.C., (2018), Numerical Simulation on Flame Propagation Characteristics of Coal Dust Explosion in Diagonal Structure Network, *Chemical Engineering Transactions*, **66**, 277-282.

Suvar M.C., Cioclea D., Arad V., Lupu C.,; Vlasin N.I., (2017), Method for improving the management of mine ventilation networks after an explosion, *Environmental Engineering and Management Journal*, **16**, 1373-1381.

Yang S.Z., Jing G.X., Cheng L., (2010), Experiment research on coal dust explosion propagation in restrained space, *Coal Science and Technology*, **38**, 35-38.